Mine Water and the Environment (2020) 39:356–368
https://doi.org/10.1007/s10230-020-00667-w

TECHNICAL ARTICLE

Groundwater Hydrogeochemical Processes and the Connectivity of Multilayer Aquifers in a Coal Mine with Karst Collapse Columns

Haitao Zhang[1] · Guangquan Xu[1] · Xiaoqing Chen[1] · Anesu Mabaire[1] · Jisheng Zhou[2] · Yanxi Zhang[2] · Gang Zhang[2] · Liang Zhu[2]

Received: 26 July 2019 / Accepted: 13 February 2020 / Published online: 24 February 2020

Abstract
Understanding groundwater hydrogeochemical processes and the connectivity of multilayer aquifers in a coal mine with karst collapse columns (KCCs) is very important for mine safety and groundwater resource management. In this study, 52 groundwater samples from the main aquifers in the Xieqiao coal mine (Anhui Province, China) were analyzed using hydrochemical, multivariate statistical methods, and stable isotope analyses. In the Permian aquifer, the main hydrogeochemical processes are halite and silicate dissolution and sulfate reduction, followed by cation exchange, while in the Carboniferous and Ordovician aquifers, the main hydrogeochemical processes are carbonate, gypsum, and halite dissolution, followed by cation exchange. This causes the hydrochemical characteristics of these two aquifers to be similar. The Permian aquifer contains less SO_4^{2-}, more HCO_3^- concentration, and a concentration ratio of SO_4^{2-} to HCO_3^- less than 0.25 due to sulfate reduction, which allows the Permian aquifer to be distinguished easily from the other two. Both hierarchical cluster and stable isotope analysis show that water samples from both aquifers appear to have been mixed via the KCCs, which may serve as a potential channel for groundwater inrush into the coal mine. These results may assist in accurately predicting potential water inrush sources in this coal mine as well as in other mines.

Keywords Major ion chemistry · Stable isotopes · Principal component analysis · Hierarchical cluster analysis · Two-component mixing models

Introduction

Groundwater is an important resource, worldwide (Wang et al. 2019). Approximately 61% of cities in China use groundwater for drinking; however, ≈ 40% (2.7 Gm^3) of groundwater in China has been affected by mining (Liang et al. 2018; Liu et al. 2017). Mining activities can influence groundwater geochemistry and the hydraulic connections of adjacent aquifers (Chen et al. 2017; Li et al. 2018; Qian et al. 2016), which may greatly reduce the accurate discrimination of inrush sources and affect mine safety. In many exploited coal mines in north China, the groundwater system is extremely complex, comprising multi-aquifers with varied hydrochemical characteristics and hydrogeochemical processes (Huang and Jian 2012). In addition, different aquifers are often connected by faults, karst collapse columns (KCCs), and other geological structures (Chen et al. 2016; Li and Wu 2019; Li et al. 2017); in particular, KCCs often function as conduits between different aquifers. According to incomplete official statistics, since the 1970s, 12 water inrush accidents have been induced by KCCs, resulting in serious loss of life and property (Gui et al. 2017). Therefore, identifying the hydrogeochemical processes and hydraulic connections of the aquifers in coal mines with KCCs can help to accurately predict potential water inrush sources and take appropriate preventive measures.

Many researchers have found that the major ions and stable isotopes in groundwater can provide geochemical information on aquifers (Cortes et al. 2016; Dehbandi et al. 2017; Li et al. 2013, 2016a; Qian et al. 2013, 2016) and thus enable evaluations of the hydrogeochemical processes and aquifer connectivity (Chen et al. 2017; Liu et al. 2017; Qian et al. 2016). For example, Qian et al. (2018) used major ion

✉ Haitao Zhang
entao0824@163.com

[1] School of Earth and Environment, Anhui University of Science and Technology, Huainan 232001, China

[2] Department of Geology and Hydrogeology, Xieqiao Coal Mine, Huainan Mining Group, Huainan 232001, China

chemistry to identify groundwater hydrochemical processes in the northeastern Huaibei Plain. Their research revealed that there were three sub-processes for the karst groundwater in this area, namely, dolomite dissolution, gypsum dissolution, and mixing. Huang and Han (2017) used stable isotopes and major chemical ions to determine the interactions between aquifers in the Sihe coal-mining area. Stable isotope ($\delta^{18}O$, $\delta^{2}H$, $\delta^{3}H$, and $\delta^{34}S$) analyses showed that the aquifers of the Taiyuan, Fengfeng, and Majigou Groups in that area have a vertical hydraulic connection.

To evaluate the hydrogeochemical processes and aquifer connectivity, several different approaches, such as hydrochemical analysis and multivariate statistical methods, have been successfully used to study regional and local groundwater systems (Belkhiri et al. 2010; Cortes et al. 2016; Li et al. 2019a; Sefie et al. 2018; Voutsis et al. 2015; Wu et al. 2014, 2019). Hydrochemical analysis techniques, such as different graphical techniques (e.g. box plots and Piper diagrams) and scatter plots, have been used widely to analyze the hydrochemical characteristics and sources of major ions (Ma et al. 2018; Zhang et al. 2016). Multivariate statistical methods, such as principal component analysis (PCA) and hierarchical cluster analysis (HCA), have been employed successfully to identify hydrogeochemical processes (Blake et al. 2016; Li et al. 2019a; Liu et al. 2017; Wu et al. 2014, 2019) and to assess aquifer connectivity (Huang and Han 2017; Qian et al. 2016). PCA is one of the most powerful methods to reduce numerous and complex datasets into a smaller number of uncorrelated components while retaining the bulk of the information (Qian et al. 2016; Voutsis et al. 2015). HCA is one of the most widely applied cluster techniques and can be used to classify water samples based on a comprehensive consideration of various hydrochemical indicators (Liu et al. 2017; Qian et al. 2016). In recent years, many researchers have shown not only that stable isotopes can identify the sources of water inrush (Guan et al. 2019; Huang et al. 2018; Jin et al. 2018) but also that its mixing models can deduce the mixing ratios of groundwater in different aquifers (Li et al. 2016b; Rambabu et al. 2018; Richards et al. 2018; Tomonaga et al. 2016). Li et al. (2016b) used a three end-member mixing model based on stable isotopes and chloride to quantify the mixing ratios between shallow groundwater and river water in the Hua County of China; this model provides a novel approach to study the hydraulic connections between different water bodies. Richards et al. (2018) used two-component mixing models based on $\delta^{2}H$ and $\delta^{18}O$ to determine the mixing ratio between shallow groundwater in the Kandal Province of Cambodia and surface water. An analysis of the mixing models indicated that shallow groundwater in this area was recharged by surface water, especially during the rainy season, and that 40–70% of the groundwater recharge comes from surface water. Thus, combining hydrochemical and multivariate statistical methods with stable isotope analyses can offer a more reasonable and scientific explanation of groundwater hydrogeochemical processes and aquifer connectivity.

The Xieqiao coal mine is a large modern coal mine with an annual output of 10 million metric tons. It is one of the three main mining bases in the Huainan coalfield, which contains ≈ 20% of the coal reserves in north China (Chen et al. 2014; Zhang et al. 2019a). However, since it was first mined in 1997, the hydrogeological conditions in this mine were not considered complex until two KCCs (KCC 1# and KCC 2#) were recently discovered in its east zone. Therefore, in this study, the hydrochemical characteristics, groundwater hydrogeochemical processes, and hydraulic connectivity of the main aquifers in the Xieqiao coal mine were analyzed using hydrochemical and multivariate statistical methods and stable isotope analyses. The research results can provide a scientific basis to identify and predict potential water inrush sources in the Xieqiao coal mine and will assist in the management and protection of groundwater resources.

Study Area

The Xieqiao coal mine is located southwest of the Huainan coal field in Anhui Province, China, with a total area of 50 km^2 (Fig. 1a). It is controlled by a semi-humid climate with seasonal monsoons. From 1981 to 2017, the annual average temperature was 15.7 °C and the annual average precipitation was 926.15 mm. The precipitation in the study area occurs primarily in June, July, and August, accounting for ≈ 50% of the total annual precipitation.

The minefield contains 25 coal-bearing layers, primarily distributed in the Permian strata. Of these, six layers consist of the main minable and stable coal seams, with an average thickness of 17.5 m; they are numbered 13-1, 11-2, 8, 6, 4-2, and 1 from the top to the bottom (Fig. 1b). Present mining activities are focused only at the top coal seams 13-1, 11-2, 8, and 6, while the lower seams. 4-2 and 1 have not yet been exploited. The formation strike of the coal mine is N 105° S and the dip direction is N 195° W, with dip angles between 5° and 15° (Fig. 1b). The main faults include F5, F6, F10, F11, F22, F202, and F206, and the small folds and faults are developed unevenly (Fig. 1). In addition, there are two KCCs in the minefield's east zone (Fig. 1b). Three-dimensional seismic exploration indicates that the lengths of KCCs #1 and #2 are 337 and 1117 m, respectively, in the Permian coal measures layer (coal seam 1) and their widths are 387 and 159 m, respectively. From the top down, the diameters of the two KCCs become increasingly larger, and both pass through the Permian coal measures, the Carboniferous limestone, and the Ordovician limestone layers. Therefore, the present study focused on the Permian fractured sandstone aquifer,

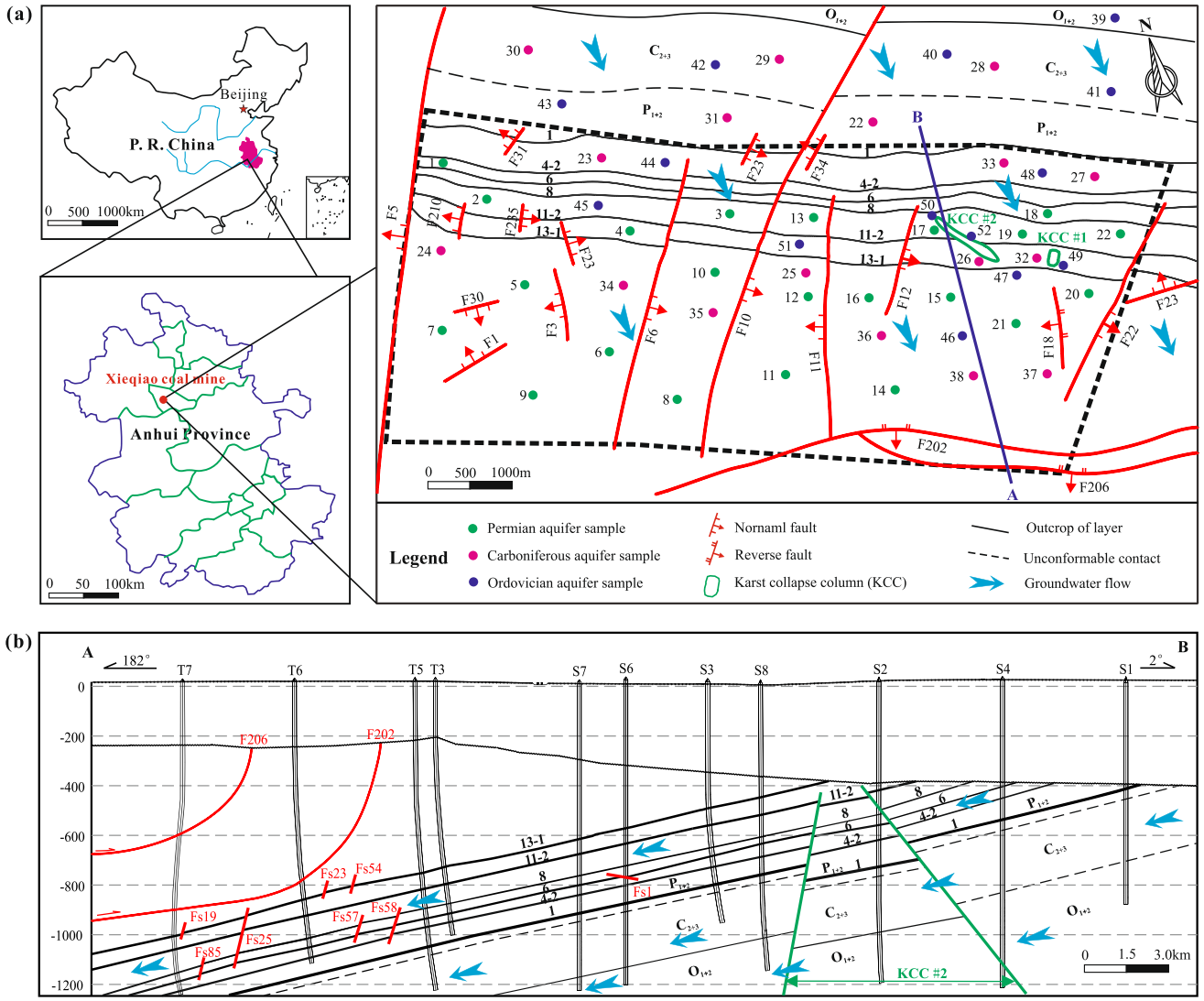

Fig. 1 General map of the studied area and the water samples position: **a** A map showing the location of the study area, with the distribution of faults, KCCs, and sampling sites within the Xieqiao coal mine; **b** Cross section of the Xieqiao coal mine along line A–B

the Carboniferous fractured-karst limestone aquifer, and the Ordovician karst limestone aquifer, referred to as the Permian, Carboniferous, and Ordovician aquifers, respectively. Groundwater from the four aquifers generally flows from north to south and from the shallow outcrop area to the deeply buried area (Fig. 1a, b). Considering the thick cover layer and poor runoff conditions, the Xieqiao minefield is deemed a stagnant zone in the regional groundwater flow field.

The Permian aquifer is ≈1000 m thick and primarily composed of medium to fine sandstone. In the thick-bedded sandstone of the main coal seams, a large number of unevenly developed fractures, often filled with calcium, are observed. The bottom of the Permian aquifer contains an aquiclude composed of mudstone and sandy mudstone, partially intercalated with fine sandstone. Because of this aquiclude, the Permian aquifer is usually not hydraulically connected to the underlying Carboniferous aquifer.

The Carboniferous aquifer is ≈120 m thick. It comprises thin-layer limestone, mudstone, sandy mudstone, sandstone, and thin coal seams. Of these, there are 12 layers of limestone, with a total average thickness of 57 m. In the thin-layer limestone, dissolution fissures and apertures are prevalent and usually filled with calcite or pyrite. The bottom aquiclude primarily contains piebald mudstone and aluminous mudstone, and it is 13–20 m thick, with an average thickness of 15 m. Therefore, the Carboniferous aquifer is generally not connected to the underlying Ordovician aquifer.

The Ordovician aquifer is 107 m thick and primarily composed of dolomitic and argillaceous limestone, with a small amount of locally interspersed mudstone. In the Ordovician

aquifer, dissolution fissures, apertures, and caves are prevalent and usually filled with calcite or mud. Its specific discharge is 0.14–2.38 L/s/m and its permeability coefficient is 0.08–0.82 m/day. A large number of pumping tests indicates that hydraulic connections between the Ordovician and Carboniferous aquifers might exist in the vicinity of KCC #1 and KCC #2.

Materials and Methods

Sampling and Laboratory Analyses

In this study, 52 water samples, including 22 samples from the Permian aquifer, 16 samples from the Carboniferous aquifer, and 14 samples from the Ordovician aquifer, were collected in Sept. 2018 in the study area (the positions of the samples are shown in Fig. 1) to test the general hydrogeochemical variables (pH, total dissolved solids [TDS], $Na^+ + K^+$, Ca^{2+}, Mg^{2+}, Cl^-, SO_4^{2-}, and HCO_3^-). In addition, 16 samples from the Carboniferous aquifer and 14 samples from the Ordovician aquifer were also tested for stable isotopes (δ^2H and $\delta^{18}O$). The samples from the Permian aquifer (coal seams 13-1, 11-2, 8, and 6) were all collected from mining tunnels, while the Carboniferous and Ordovician aquifer samples were collected from pumping test wells.

When sampling, all samples were filtered on-site through 0.45 μm membranes. The 52 samples for the cation analysis were stored in 550 mL polypropylene bottles and acidified to $pH \leq 2$ using HNO_3. The duplicate set of 52 samples for the anion analysis was not acidified. While in the field, the pH was measured on-site using a portable tester (HI8424, $pH \pm 0.01$, Italy). The concentrations of major ions, such as Cl^-, SO_4^{2-}, and HCO_3^-, were analyzed via ion chromatography (Dionex 120), and Ca^{2+}, Mg^{2+}, Na^+, and K^+ were analyzed by inductively coupled plasma-atomic emission spectrometry (Thermo Fisher Scientific). As the K^+ concentration in the water samples was very small, the Na^+ and K^+ concentrations were analyzed as a sum ($Na^+ + K^+$). All the samples were analyzed at the Water Quality Testing Center at the Anhui University of Science and Technology, Huainan, China, within 24 h of collection. The PHREEQC 3.0 software was used to calculate the saturation index and the charge balance of each sample. All water samples were in a perfect charge balance, with error percentages of < 5% (Table 1).

The hydrogen and oxygen isotopes of the samples were analyzed at the School of Earth and Space Sciences, University of Science and Technology of China, Hefei, China, within 3 days of collection. The hydrogen isotopes (δ^2H) were measured using the zinc reaction method, and the oxygen isotopes ($\delta^{18}O$) were measured using the oxygen and carbon dioxide balance method, with a MAT252 isotope mass spectrometer. The results of the hydrogen and oxygen isotope (δ^2H and $\delta^{18}O$) tests were examined in comparison with the Vienna standard mean ocean water standard and their ranges were ± 0.2% and ± 0.1%, respectively.

Three aquifer cores were collected and tested to predict the potential minerals. X-ray powder diffraction (XRD) and scanning electron microscope (SEM) tests were conducted using SmartLab SE XRD (Japan) and FlexSEM1000 SEM (Japan) devices, respectively, both at the Testing Center of the Anhui University of Science and Technology, Huainan, China. The three aquifer cores are available to be tested and the predicted potential minerals are listed in Table 2.

Table 1 Summary statistics of hydrogeochemical variables

Variables	Permian aquifer (n = 22)				Carboniferous aquifer (n = 16)				Ordovician aquifer (n = 14)			
	Min	Max	Mean	C_v (%)	Min	Max	Mean	C_v (%)	Min	Max	Mean	C_v (%)
K^++Na^+ (mg/L)	573.14	1061.68	686.52	16.40	689.42	1031.53	913.05	10.92	442.78	882.05	789.94	14.85
Ca^{2+} (mg/L)	2.81	19.84	12.60	46.43	3.90	56.99	44.24	28.04	3.41	50.22	35.74	47.62
Mg^{2+} (mg/L)	1.09	16.42	9.30	61.91	2.37	24.13	13.35	49.82	1.78	22.84	15.50	40.51
Cl^- (mg/L)	271.57	817.55	596.97	19.57	759.05	1277.50	1057.46	12.66	556.09	1143.60	939.13	15.88
SO_4^{2-} (mg/L)	3.29	182.96	53.11	118.73	220.08	567.23	401.21	19.45	164.86	442.15	283.86	28.07
HCO_3^- (mg/L)	439.14	1679.82	764.74	40.72	43.68	462.79	281.23	32.42	111.96	345.25	275.55	26.84
TDS (mg/L)	1487.60	2597.44	1759.56	14.21	1942.52	2907.29	2578.56	9.61	1281.49	2481.54	2218.20	14.62
Error (%)	0.12	2.40	0.81	3.56	0.56	3.60	1.93	7.87	0.13	2.92	1.73	5.64
Eh (mV)	306.67	345.21	324.32	5.16	316.62	386.75	345.67	8.63	376.25	398.31	386.73	4.62
pH	8.01	9.17	8.11	3.86	8.06	9.08	8.33	3.62	8.02	9.66	8.73	6.97
$\delta^{18}O$ (‰)	–	–	–	–	− 7.68	− 3.34	− 5.36	22.06	− 9.97	− 7.01	− 8.93	11.11
δ^2H (‰)	–	–	–	–	− 59.39	− 25.00	− 43.77	24.15	− 88.88	− 55.49	− 74.66	13.64

Table 2 XRD and SEM tests results of the cores samples from different aquifers

Aquifers	Minerals compositions calculated with XRD test	Potential hydrogeochemical processes	Remarks
Permian aquifer	Mainly quartz with kaolinite and less pyrite	Minerals dissolution	Typical sandstone
Carboniferous aquifer	Calcite, gypsum, quartz and kaolinite dominates with less dolomite	Carbonates system and cation exchange	Typical limestone and clay minerals
Ordovician aquifer	Calcite, dolomite and gypsum with less kaolinite	Carbonates system	Typical limestone

Analytical Methods

Multivariate Statistical Analyses

In this study, PCA and HCA were both used to analyze the groundwater geochemistry data using the SPSS 19.0 statistical software. PCA was employed to identify the main processes controlling groundwater geochemistry (Blake et al. 2016; Li et al. 2019a; Liu et al. 2017; Qian et al. 2016; Wu et al. 2014), and the variables included in the PCA were $Na^+ + K^+$, Ca^{2+}, Mg^{2+}, HCO_3^-, Cl^-, and SO_4^{2-}. The varimax rotation method was used to maximize the differences between the extracted components, and the highly loaded components with eigenvalues > 1.0 were obtained (Davis 2005). These had a total cumulative variance greater than 80% based on the Kaiser criterion (Kaiser 1960) and the screen plot elbow point approach (Cattell 1966), were selected as the principal components (PCs). The PCA results were examined in terms of the PC loading scores, sometimes referred to as factor scores (Shaw 2003).

HCA was used to classify similar water samples into separate groups based on the comprehensive consideration of various hydrochemical indicators (e.g. $Na^+ + K^+$, Ca^{2+}, Mg^{2+}, HCO_3^-, Cl^-, and SO_4^{2-}). The same group (or cluster) contains samples that are similar to each other, but different from other samples (Liu et al. 2017; Voutsis et al. 2015). In this study, the Ward method and the Euclidean distance were selected for the linkage rules and the geometric distance between the samples, respectively, because they have been shown to be applicable to hydrogeochemical studies (Qian et al. 2016).

Stable Isotope Mixing Models

Stable isotope mixing models are often used to identify water inrush sources and determine the mixing ratios of different water sources (Binet et al. 2016; Qian et al. 2013, 2014; Rambabu et al. 2018; Richards et al. 2018; Tomonaga et al. 2016). The mixing ratio of a water source is estimated using two-component mixing models with end members representing the δ^2H and $\delta^{18}O$ values of two completely different aquifers (e.g., the Carboniferous and Ordovician aquifers). The two-component mixing models were calculated using Eqs. (1) and (2):

$$M_{MW,\delta^2H} = \frac{\delta^2H_{MW} - \delta^2H_{EMB}}{\delta^2H_{EMA} - \delta^2H_{EMB}} \quad (1)$$

$$M_{MW,\delta^{18}O} = \frac{\delta^{18}O_{MW} - \delta^{18}O_{EMB}}{\delta^{18}O_{EMA} - \delta^{18}O_{EMB}} \quad (2)$$

where the relative extent of the water source mixing (M) of a groundwater sample based on δ^2H or $\delta^{18}O$ is $M_{MW,\,\delta2H}$ or $M_{MW,\,\delta18O}$, respectively; and the δ^2H and $\delta^{18}O$ values of the mixing water and A (e.g. the Carboniferous aquifer) and B (e.g. the Ordovician aquifer) end members are measured.

Results and Discussion

General Hydrochemical Characteristics

The results of the hydrochemical analysis are listed in Table 1. The statistical results indicate that all the water samples were alkaline and weakly saline, with pH > 8 and TDS > 1 g/L. Relative to the other two aquifers, the Permian aquifer has lower TDS and SO_4^{2-} concentrations and a higher HCO_3^- concentration (Table 1). Liu et al. (2019) found that this phenomenon is related to desulfurization, which reduces the TDS and SO_4^{2-} concentrations, but increases the HCO_3^- concentration.

The coefficient of variation (C_v) is an indicator of the degree of data dispersion. When the C_v is less than 10%, the variable has weak variation; when the C_v is between 10% and 100%, the variable has moderate variation; and when the C_v is larger than 100%, the variable has strong variation (Qian et al. 2018). As shown in Table 1, most of the variables have moderate or even strong variations, indicating that the groundwater geochemical formation mechanism in this area is complex, which highlights the necessity of studying the hydrochemical characteristics and groundwater hydrogeochemical processes in this system.

Piper diagrams can be used to analyze the hydrochemical characteristics (Qian et al. 2016; Zhang et al. 2019b).

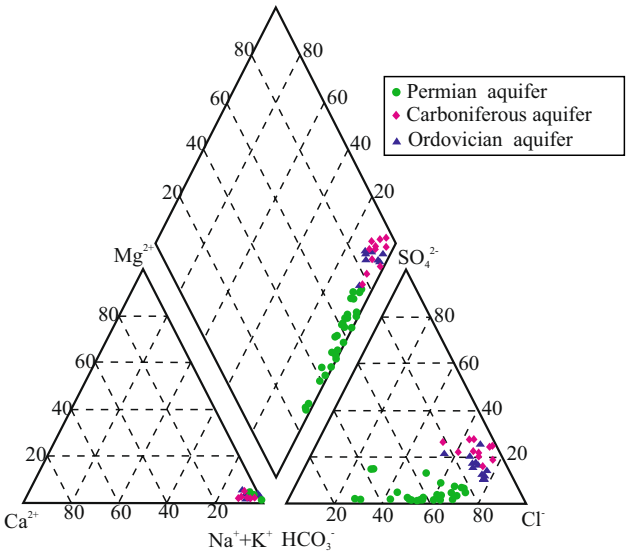

Fig. 2 Piper diagram of the chemical type of water samples form different aquifers

As seen in Fig. 2, the water samples from the three aquifers are all dominated by alkali metal ions ($Na^+ + K^+$) and the milliequivalent percentage of $Na^+ + K^+$ exceeds 80%, suggesting that the study area has been in a relatively closed environment (Xu et al. 2015). As for the anions, most of the water samples from the three aquifers have a high Cl^- concentration; some water samples from the Permian aquifer also had high HCO_3^- concentrations (Fig. 2). Therefore, the main chemical type of the Carboniferous and Ordovician aquifers is the Na + K–Cl type, while the Permian aquifer has two primary chemical types: Na + K–Cl and Na + K–Cl–HCO_3.

Box plots (Fig. 3a–f) are usually used to analyze changes in the concentrations of major ions (Zhang et al. 2016). In Fig. 3e, f, the Permian aquifer is seen to have a low SO_4^{2-} concentration and a high HCO_3^- concentration. Meanwhile, the concentration ratio of SO_4^{2-} to HCO_3^- in the Permian aquifer is less than 0.25, while the same ratio for the Carboniferous and Ordovician aquifers is greater than 0.25 (Fig. 4a). Thus, the concentration ratio of SO_4^{2-} to HCO_3^- can easily be used to distinguish water from the Permian aquifer from water from the other aquifers. As shown in Figs. 2 and 3a–f, the concentrations of $Na^+ + K^+$, Ca^{2+}, Mg^{2+}, Cl^-, HCO_3^-, and SO_4^{2-} in the Carboniferous and Ordovician aquifers are similar, suggesting that the groundwater in these two aquifers has similar hydrochemical characteristics and hydrogeochemical processes (Chen et al. 2017; Qian et al. 2016). Therefore, it is necessary to analyze the major hydrogeochemical processes and aquifer connectivity before the sources of the two aquifers can be identified accurately.

Evidence of Major Hydrogeochemical Processes

Mineral Phase Analysis

The results of the XRD and SEM tests (Table 2) indicate that the potential reactants for the water–rock reactions include carbonate minerals, such as calcite and dolomite; crystal minerals, such as gypsum and quartz; and clay minerals, such as kaolinite. In this study, pyrite was not considered, although the XRD and SEM tests indicate that this mineral may exist in the Permian aquifer because the amount of pyrite detected is too small to influence the major hydrogeochemical processes. The major ion compositions indicate major reactants, such as calcite, dolomite, and sulfate, along with some sodium minerals (e.g. salt rock and silicate) and gypsum. As the clay layers contain the most important aquitard materials, cation exchange can also be assessed in the three aquifers.

Source Analysis of Ca^{2+}, Mg^{2+}, HCO_3^-, and SO_4^{2-}

Many studies have shown that Ca^{2+}, Mg^{2+}, and HCO_3^- in groundwater are derived primarily from carbonate mineral dissolution (Chen et al. 2017; Li et al. 2019b; Liu et al. 2017; Qian et al. 2018). When $\rho(HCO_3^-)/\rho(Ca^{2+}) = 1$, it means that HCO_3^- and Ca^{2+} could be formed by the single dissolution of calcite (Eq. 3). When $\rho(HCO_3^-)/\rho(Ca^{2+}) = 4$, it means that HCO_3^- and Ca^{2+} could be formed by the single dissolution of dolomite (Eq. 4). As shown in Fig. 4b, the lines $y = 2x$ and $y = 4x$ divide the entire area into three zones. The lower zone shows an HCO_3^- deficiency, and only one water sample from the Carboniferous aquifer falls in this zone. The middle zone shows an HCO_3^- concentration increase, representing a combination of calcite and dolomite dissolution or calcite dissolution and cation exchange (Liu et al. 2017). There are only three water samples from the Carboniferous aquifer in the middle zone (Fig. 4b).

$$\text{Calcite: } CaCO_3 + CO_2(g) + H_2O \rightarrow Ca^{2+} + 2HCO_3^- \quad (3)$$

$$\text{Dolomite: } CaMg(CO_3)_2 + 2CO_2(g) + 2H_2O \rightarrow Ca^{2+} + Mg^{2+} + 4HCO_3^- \quad (4)$$

If calcite and dolomite dissolution are the major origins of Ca^{2+}, Mg^{2+}, and HCO_3^-, then the upper zone must be involved with cation exchange, resulting in a HCO_3^- concentration $> 4 \times Ca^{2+}$ (Liu et al. 2017). In Fig. 4b, most water samples from the Carboniferous and Ordovician aquifers are characterized by cation exchange. However, in the Permian aquifer, clay and crystal minerals are the major origins of the groundwater; therefore, the upper zone (Fig. 4b) may

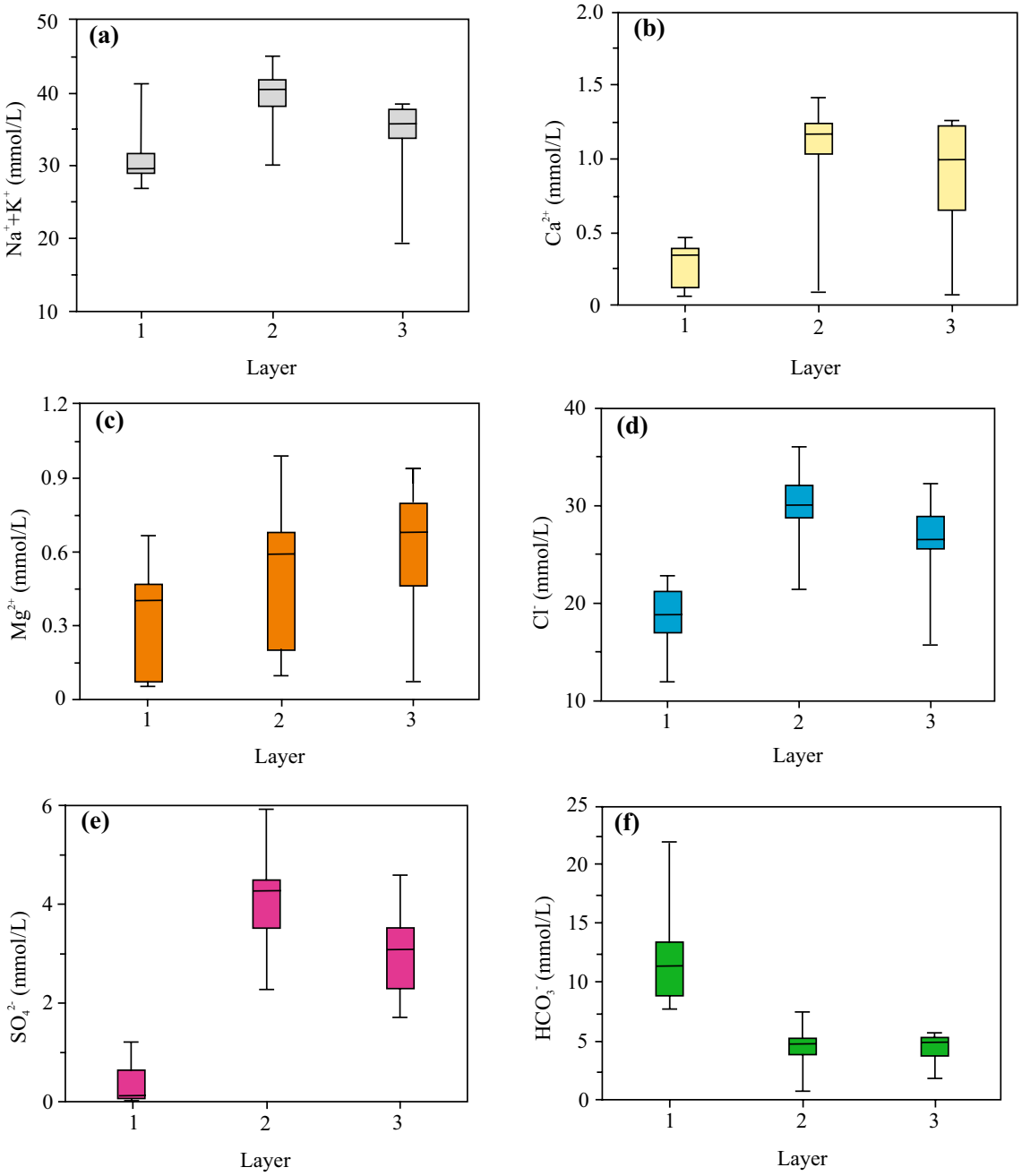

Fig. 3 Boxplots of major hydrochemical parameters form different aquifers. Layer ID: 1-Permian aquifer, 2-Carboniferous aquifer, 3-Ordovician aquifer

be involved with silicate dissolution (Eq. 5) and/or sulfate reduction (Eq. 6) and/or cation exchange (Qian et al. 2016).

$$\text{Silicate: } (Na,K)_2Al_2Si_6O_6 + 3H_2O + 2CO_2 \rightarrow 2(Na,K)^+ + 2HCO_3^- + H_4Al_2Si_6O_6 + 4SiO_2 \quad (5)$$

$$\text{Desulfidation: } SO_4^{2-} + 2C + 2H_2O \rightarrow H_2S\uparrow + 2HCO_3^- \quad (6)$$

Figure 4c provides evidence of gypsum in the three aquifers, with correlation coefficients close to 1 (Ca^{2+}, $R^2 = 0.73$; SO_4^{2-}, $R^2 = 0.71$). In Fig. 4d, the values of $[\rho(Ca^{2+}) + \rho(Mg^{2+})]/\rho(SO_4^{2-})$ in the Carboniferous and Ordovician aquifers are close to 1, indicating that the SO_4^{2-} in these aquifers is derived primarily from gypsum dissolution (Eq. 7). Conversely, in the Permian aquifer, the values of $[\rho(Ca^{2+}) + \rho(Mg^{2+})]/\rho(SO_4^{2-})$ are much less

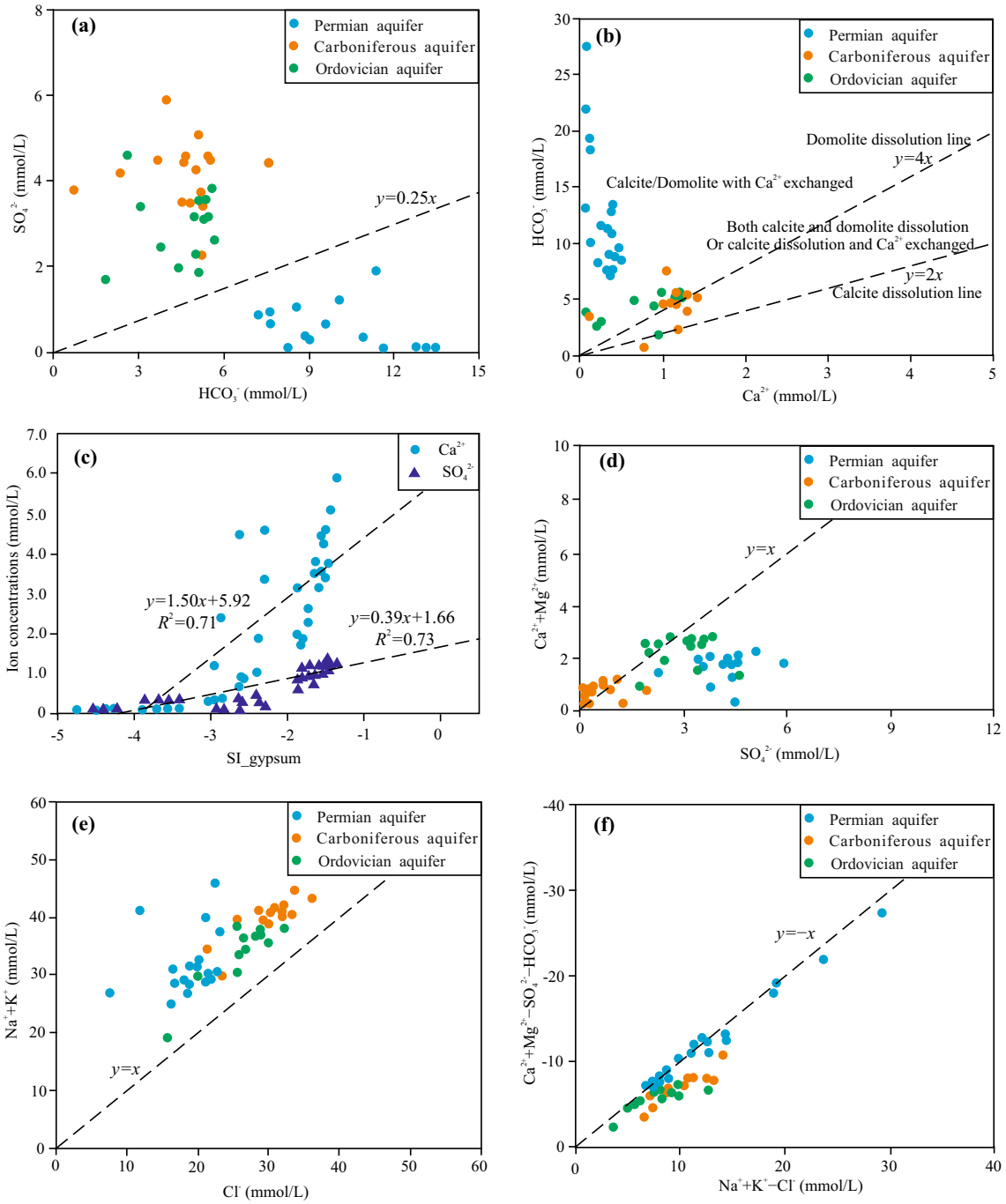

Fig. 4 Scatter plots of major ions: **a** scatter plot of SO_4^{2-} and HCO_3^-; **b** scatter plot of HCO_3^- and Ca^{2+}; **c** gypsum dissolution evidence in the three aquifers; **d** scatter plot of Ca^{2+}+Mg^{2+} and SO_4^{2-}; **e** scatter plot of $Na^+ + K^+$ and Cl^-; **f** scatter plot of $Ca^{2+}+Mg^{2+}$-SO_4^{2-}-HCO_3^- vs $Na^+ + K^+$-Cl^-

than 1, suggesting that gypsum dissolution is not the only source of SO_4^{2-} and that cation exchange may be taking place.

$$\text{Gypsum: } CaSO_4 \cdot 2H_2O \rightarrow Ca^{2+} + SO_4^{2-} + 2H_2O \quad (7)$$

Source Analysis of $Na^+ + K^+$ and Cl^-

The concentrations of $Na^+ + K^+$ and Cl^- are relatively stable in groundwater; therefore, $\rho(Na^+ + K^+)/\rho(Cl^-)$ is used commonly to reveal the source of $Na^+ + K^+$. When

$\rho(Na^+ + K^+)/\rho(Cl^-) = 1$, it means that the $Na^+ + K^+$ and Cl^- in the groundwater are derived from saline rock dissolution (Chen et al. 2017; Li et al. 2016c). As seen in Fig. 4e, the values in the three aquifers show that $\rho(Na^+ + K^+)/\rho(Cl^-) > 1$, indicating that, in addition to halite dissolution (Eq. 8), strong cation exchange must be taking place in the three aquifers.

$$\text{Halite: } Na^+(K^+)Cl \rightarrow Na^+(K^+) + Cl^- \quad (8)$$

Considering that Ca^{2+}, Mg^{2+}, and $Na^+ + K^+$ arise from mineral dissolution, the ratio of $\rho(Ca + Mg–SO_4–HCO_3)/\rho(Na^+ + K^+–Cl^-)$ in mol/L will be constant at 1:1 (Chen et al. 2017; Li et al. 2016d). The scatter distribution in Fig. 4f in the lower right zone also indicates that cation exchange occurs in the solutions (Voutsis et al. 2015). In Carboniferous and Ordovician aquifers, the ratio of $\rho(Na^+ + K^+–Cl^-)/\rho(Ca + Mg–SO_4–HCO_3)$ of some samples is more than 1 (Fig. 4f), which may be related to strong cation exchange. Cation exchange (Eq. 9) causes the concentration of $Na^+ + K^+$ to increase while decreasing the concentrations of Ca^{2+} and Mg^{2+}.

$$Na^+(K^+)(\text{rock}) + Ca^{2+}(Mg^{2+})(\text{water}) \rightarrow Na^+(K^+)(\text{water}) + Ca^{2+}(Mg^{2+})(\text{rock}) \quad (9)$$

Principal Component Analysis

The correlation matrix (Table 3) shows that $Na^+ + K^+$ has a good positive correlation with Cl^- and HCO_3^- because of the dissolution of halite and silicate; however, $Na^+ + K^+$ is negatively correlated with Ca^{2+} and Mg^{2+}, which is a typical feature of cation exchange (Chen et al. 2017). The correlation coefficient between Ca^{2+} and Mg^{2+} is 0.954, suggesting the existence of a good carbonate system (Liu et al. 2017). In addition, Ca^{2+} is positively correlated with SO_4^{2-}, which relates to gypsum dissolution, while SO_4^{2-} has a negative correlation with HCO_3^-, which, as mentioned above, is a typical feature of sulfate reduction (Qian et al. 2016).

Using the Kaiser criterion and scree plot method (Liu et al. 2017; Voutsis et al. 2015), PCA obtained two valid PCs (PC1 and PC2) with eigenvalues > 1.0 and a total cumulative variance > 81%, as shown in Table 3. PC1 explained 49.45% of the total variance and was characterized by high positive loading for $Na^+ + K^+$, Ca^{2+}, Mg^{2+}, and SO_4^{2-}, but negative loading for HCO_3^- (Table 4; Fig. 5a), corresponding to the dissolution of minerals (e.g., calcite, dolomite, and gypsum) and sulfate reduction, respectively. PC2 explained 31.99% of the total variance and had high positive loading for $Na^+ + K^+$, Cl^-, and HCO_3^-, but weakly negative loading for Ca^{2+} and Mg^{2+} (Table 4; Fig. 5a), which represents silicate and halite dissolution and cation exchange, respectively.

As seen in Fig. 5b, all the water samples from the Permian aquifer fall in the second and third quadrants, showing high loading scores for HCO_3^-, $Na^+ + K^+$, and Cl^-, but low loading scores for Ca^{2+}, Mg^{2+}, and SO_4^{2-}, which indicates that they are influenced primarily by halite and silicate dissolution and sulfate reduction, followed by cation exchange. The samples from the Ordovician aquifer fall primarily in the first and fourth quadrants (Fig. 5b), corresponding to relative high loading scores for Ca^{2+}, Mg^{2+}, and SO_4^{2-}, but low loading scores for HCO_3^-, $Na^+ + K^+$, and Cl^-, which shows that they are influenced primarily by the dissolution of carbonate, gypsum, and halite, followed by cation exchange. In comparison, the samples from the Carboniferous aquifer are located primarily in the first quadrant (Fig. 5b), showing

Table 4 Correlation matrix of the species in all samples

Species	Coefficients of PC1	Coefficients of PC2
$Na^+ + K^+$	**0.628***	**0.774***
Ca^{2+}	**0.877***	− 0.102
Mg^{2+}	**0.719***	− 0.245
Cl^-	0.135	**0.674***
SO_4^{2-}	**0.883***	0.025
HCO_3^-	**− 0.746***	**0.543***
Eigenvalue	3.891	1.096
% of variance explained	49.45	31.99
% of cumulative variance	49.45	81.44

Significant factors are in bold font

*Correlation is significant at the 0.01 level

Table 3 Correlation matrix of the species in all samples

Correlation	$Na^+ + K^+$	Ca^{2+}	Mg^{2+}	Cl^-	SO_4^{2-}	HCO_3^-
$Na^+ + K^+$	1					
Ca^{2+}	**− 0.636***	1				
Mg^{2+}	**− 0.503***	**0.954***	1			
Cl^-	**0.835***	0.242	0.325	1		
SO_4^{2-}	0.175	**0.758***	0.305	0.198	1	
HCO_3^-	**0.709***	**− 0.653***	**− 0.596***	− 0.181	**− 0.468***	1

Significant factors are in bold font

*Correlation is significant at the 0.01 level

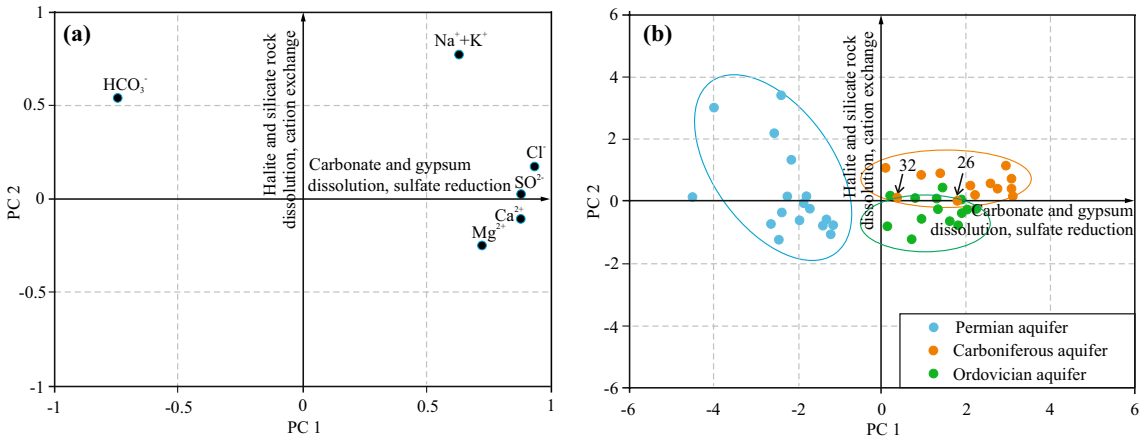

Fig. 5 PCs analysis plots: **a** loadings plot for PC1 and PC2; **b** scores plot for PC1 and PC2

high loading scores for Ca^{2+}, Mg^{2+}, $SO_4{}^{2-}$, $Na^+ + K^+$, and Cl^-, but low loading scores for $HCO_3{}^-$, which indicates that they are primarily influenced by the dissolution of carbonate, gypsum, and halite, followed by cation exchange.

Notably, as seen in Fig. 5b, two water samples (26 and 32) from the Carboniferous aquifer fall within the range of the Ordovician aquifer samples and are both located near KCC #1 and KCC #2, as shown in Fig. 1. This suggests that these two water samples might reflect mixing via the two KCCs. To verify this hypothesis, HCA and stable isotope analyses were both used to identify the groundwater sources and determine their mixing ratios.

Evidence of Aquifer Connectivity

Hierarchical Cluster Analysis

Using the Ward method and Euclidean distance (Liu et al. 2017; Qian et al. 2016), HCA yielded optimum distinct groups, which are given as a dendrogram (Fig. 6). As shown in Fig. 6, the phonon line of 5.0 divides the water samples into two clusters: Cluster 1 consists of G1 and G2 that have similar hydrochemical characteristics, while Cluster 2 consists of G3, G4, and G5, which demonstrate similar hydrochemical characteristics. Cluster 2 is further subdivided into two sub-clusters: one of the sub-clusters consists of G3 and the other of G4 and G5. In Cluster 1, G1 and G2, showing lower concentrations of $SO_4{}^{2-}$ but higher concentrations of $HCO_3{}^-$, include all of the water samples from the Permian aquifer. Cluster 1 (G1 and G2) is separate from Cluster 2 (G3, G4, and G5), suggesting that the Permian aquifer is relatively isolated, with stable hydrogeochemical characteristics, and that no hydraulic connection exists between the Permian aquifer and the underlying Carboniferous and Ordovician aquifers under natural conditions. Conversely, G4 and G5 in Cluster 2, both have higher concentrations of $SO_4{}^{2-}$ but lower concentrations of $HCO_3{}^-$, primarily water samples from the Ordovician and Carboniferous aquifers, respectively, indicating that the overall hydrochemical characteristics of these two aquifers are similar, which is consistent with the results of the hydrochemical characteristic analysis. In Cluster 2, G3 consists of two water samples (26

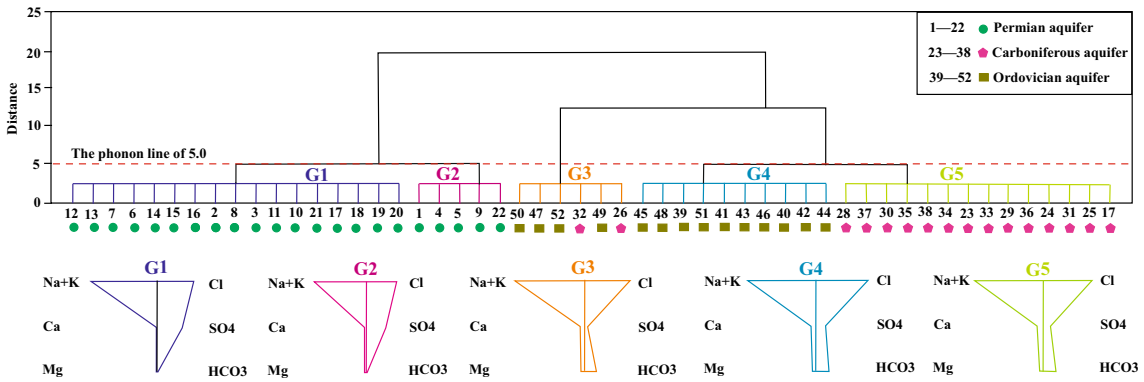

Fig. 6 Dendrogram of HCA result

and 32) from the Carboniferous aquifer and four (47, 49, 50, and 52) from the Ordovician aquifer, and the six samples are all distributed near KCC #1 and KCC #2 (Fig. 1a). Combined with the PCA and HCA results, it is speculated that the six samples reflect mixing via the KCCs or its surrounding fractures.

Stable Isotope Analyses

The local meteoric water line (LMWL) often serves as a baseline for groundwater stable isotope analyses (Chen et al. 2013; Huang and Han 2017). Accordingly, this study used the LMWL ($\delta^2H = 7.9 \times \delta^{18}O + 8.2$) (Ge et al. 2014) as a reference. Figure 7 shows that the (δ^2H, $\delta^{18}O$) points for the Carboniferous and Ordovician aquifers are all below the LMWL and lie in three regions (R1–R3). R1, consisting primarily of (δ^2H, $\delta^{18}O$) points from the Carboniferous aquifer, is located to the lower right of the LMWL line (Fig. 7). R3 consists of primarily (δ^2H, $\delta^{18}O$) points from the Ordovician aquifer and is located to the lower left of the LMWL line (Fig. 7) because of ^2H and ^{18}O drifts. R2 lies between R1 and R3 and consists of the same samples as G3 in the preceding paragraph, confirming that these water samples must reflect mixing (Binet et al. 2016).

To avoid cross-effects between the water samples, this study selected the mean values of δ^2H and $\delta^{18}O$ in the R1 water samples as the end-number values for the Carboniferous aquifer and the mean values of δ^2H and $\delta^{18}O$ in the R3 water samples as the end-number values for the Ordovician aquifer. Using Eqs. (1) and (2), the mixing ratios $M_{MW,\,\delta 2H}$, $M_{MW,\,\delta 18O}$, and $M_{MW,\,aver}$ of water samples 26, 32, 47, 49, 50, and 52 were calculated. Table 5 shows that the mixing ratios of these six water samples are all close to 50%, reconfirming that these samples reflect mixing (Richards et al. 2018; Tomonaga et al. 2016). With their developed fractures and high water yields, KCC #1 and KCC #2 could serve as water-conducting channels for water inrush. Therefore, it is necessary to pay close attention to these KCCs when mining the lower coal seams (i.e. coal seams 4-2 and 1) to avoid water inrush from the lower Carboniferous and Ordovician aquifers through the KCCs and their surrounding fractures.

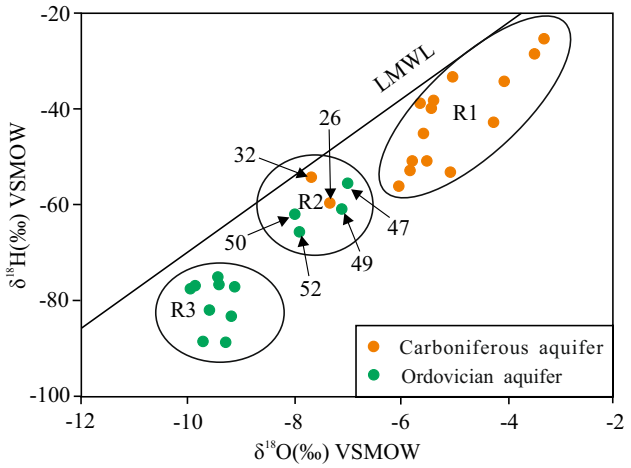

Fig. 7 δ^2H versus $\delta^{18}O$ plot of stable isotope composition of water samples. The global meteoric water line (LMWL) is $\delta^2H = 7.9 \times \delta^{18}O + 8.2$

Conclusions

Hydrochemical and multivariate statistical methods, and stable isotope analyses were used to identify the groundwater hydrogeochemical processes and aquifer connectivity in the Xieqiao coal mine. The following conclusions were drawn:

1. The Permian aquifer has a low SO_4^{2-} concentration and a high HCO_3^- concentration because of sulfate reduction, and the concentration ratio of SO_4^{2-} to HCO_3^- in the Permian aquifer is less than 0.25, allowing the Permian aquifer to be easily distinguished from the Carboniferous and Ordovician aquifers.
2. In the Permian aquifer, the main hydrogeochemical processes are dissolution of halite and silicate and sulfate reduction, followed by cation exchange. In the Carboniferous and Ordovician aquifers, the main hydrogeochemical processes are dissolution of carbonate, gypsum, and halite, followed by cation exchange, which causes the

Table 5 Results of mixing ratio of the six water samples

Sample ID	Aquifer	δ^2H (‰)	$\delta^{18}O$ (‰)	$M_{MW,\,\delta 2H}$ (%)	$M_{MW,\,\delta 18O}$ (%)	$M_{MW,\,aver}$ (%)
26	Carboniferous aquifer	− 59.39	− 7.35	54.27	48.31	51.29
32		− 54.08	− 7.68	68.17	40.90	54.53
47	Ordovician aquifer	− 62.04	− 8.01	52.67	74.00	63.34
49		− 65.74	− 7.91	62.36	71.50	66.93
50		− 55.49	− 7.01	35.52	49.00	42.26
52		− 60.80	− 7.12	49.42	51.75	50.59

$M_{MW,\,\delta 2H}$ is the mixing ratio calculated by the value of δ^2H, $M_{MW,\,\delta 18O}$ is the mixing ratio calculated by the value of $\delta^{18}O$, and M_{MW} is the average value of $M_{MW,\,\delta 2H}$ and $M_{MW,\,\delta 18O}$

hydrochemical characteristics of the two aquifers to be similar.

3. Both HCA and stable isotope analyses show that two water samples from the Carboniferous aquifer and the four from the Ordovician aquifer reflect mixing via the KCCs, which may serve as a potential channel for groundwater inrush into the coal mine.

Acknowledgements This paper was supported by the National Natural Science Foundation of China (41572147) and the China Scholarship Council (201908340093). We also express our gratitude to the suggestions from Prof. Hongbin Zhan at Texas A&M University, and from Prof. Jiazhong Qian at Hefei University of Technology.

References

Belkhiri L, Boudoukha A, Mouni L, Baouz T (2010) Application of multivariate statistical methods and inverse geochemical modeling for characterization of groundwater—a case study: Ain Azel plain (Algeria). Geoderma 159(3):390–398. https://doi.org/10.1016/j.geoderma.2010.08.016

Binet S, Joigneaux E, Pauwels H, Alberic P, Flehoc Ch, Bruand A (2016) Water exchange, mixing and transient storage between a saturated karstic conduit and the surrounding aquifer: groundwater flow modeling and inputs from stable water isotopes. J Hydrol 544:278–289. https://doi.org/10.1016/j.jhydrol.2016.11.042

Blake S, Henry T, Murray J, Flood R, Muller MR, Jones AG, Rath V (2016) Compositional multivariate statistical analysis of thermal groundwater provenance: a hydro–geochemical case study from Ireland. Appl Geochem 75:171–188. https://doi.org/10.1016/j.apgeochem.2016.05.008

Cattell RB (1966) The scree test for the number of factors. Multivar Behav Res 1(2):245–276

Chen S, Gui HR, Sun LH (2013) Hydro-geochemical and isotopic characterization of the deep groundwater from coal bearing in Mining district, Northern Anhui Province. China. Water Pract Technol 8(3–4):330–341. https://doi.org/10.2166/wpt.2013.033

Chen J, Liu GJ, Li H, Wu B (2014) Mineralogical and geochemical responses of coal to igneous intrusion in the Pansan coal mine of the Huainan coalfield, Anhui, China. Int J Coal Geol 124:11–35. https://doi.org/10.1207/s15327906mbr0102_10

Chen L, Feng X, Xie W, Xu DQ (2016) Prediction of water-inrush risk areas in process of mining under the unconsolidated and confined aquifer: a case study from the Qidong coal mine in China. Environ Earth Sci 75(8):706. https://doi.org/10.1007/s12665-016-5533-5

Chen LW, Xu DQ, Yin XX, Xie WP, Zeng W (2017) Analysis on hydrochemistry and its control factors in the concealed coal mining area in North China: a case study of dominant inrush aquifers in Suxian mining area. J China Coal Soc 42(4):996–1004 **(in Chinese)**

Cortes JE, Muñoz LF, Gonzalez CA, Niño JE, Polo A, Suspes A, Trujillo HL (2016) Hydrogeochemistry of the formation waters in the San Francisco field, UMV basin, Colombia—a multivariate statistical approach. J Hydrol 539:113–124. https://doi.org/10.1016/j.jhydrol.2016.05.010

Davis JC (2005) Statistics and data analysis in geology. Biometrics 44:526–552

Dehbandi R, Moore F, Keshavarzi B, Abbasnejad A (2017) Fluoride hydrogeochemistry and bioavailability in groundwater and soil of an endemic fluorosis belt, central Iran. Environ Earth Sci 76(4):177. https://doi.org/10.1007/s12665-017-6489-9

Ge T, Chu TT, Liu GJ, Fan X, Wu D (2014) Characterisics of hydrogen and oxygen isotopes of deep ground water in the Panxie mining area in Huainan Coalfield. J China Mar Sci Technol 44(2):112–118 **(in Chinese)**

Guan ZL, Jia ZF, Zhao ZQ, You QY (2019) Identification of inrush water recharge sources using hydrochemistry and stable isotopes: a case study of Mindong No. 1 coal mine in north-east Inner Mongolia, China. J Earth Syst Sci 128(200):2–12. https://doi.org/10.1007/s12040-019-1232-4

Gui H, Xu JP, Zhang D (2017) Relationship between hydraulic conductivity of karst collapse column and its surrounding lithology. Environ Earth Sci 76(5):2–13. https://doi.org/10.1007/s12665-017-6541-9

Huang P, Han S (2017) Study of multi–aquifer groundwater interaction in a coal mining area in China using stable isotopes and major–ion chemical data. Environ Earth Sci 76(1):2–10. https://doi.org/10.1007/s12665-016-6310-1

Huang PH, Jian SC (2012) Recharge sources and hydrogeochemical evolution of groundwater in the coal–mining district of Jiaozuo, China. Hydrogeol J 20:739–754. https://doi.org/10.1007/s10040-012-0836-4

Huang X, Wang GC, Liang XY, Cui LF, Ma L, Xu QY (2018) Hydrochemical and stable Isotope (δD and $\delta^{18}O$) characteristics of groundwater and hydrogeochemical processes in the Ningtiaota Coalfield, northwest China. Mine Water Environ 37(1):119–136. https://doi.org/10.1007/s10230-017-0477-x

Jin Z, Zheng Q, Zhu C, Wang Y, Cen JR, Li FL (2018) Contribution of nitrate sources in surface water in multiple land use areas by combining isotopes and a Bayesian isotope mixing model. Appl Geochem 93:10–19. https://doi.org/10.1016/j.apgeochem.2018.03.014

Kaiser HF (1960) The application of electronic computers to factor analysis. Educ Psychol Meas 20(20):141–151

Li B, Wu Q (2019) Catastrophic evolution of water inrush from a water-rich fault in front of roadway development: a case study of the Hongcai coal mine. Mine Water Environ 38(2):421–430. https://doi.org/10.1007/s10230-018-00584-z

Li P, Qian H, Wu J, Zhang Y, Zhang H (2013) Major ion chemistry of shallow groundwater in the Dongsheng coalfield, Ordos Basin, China. Mine Water Environ 32(3):195–206. https://doi.org/10.1007/s10230-013-0234-8

Li P, Zhang Y, Yang N, Jing L, Yu P (2016a) Major ion chemistry and quality assessment of groundwater in and around a mountainous tourist town of China. Expo Health 8(2):239–252. https://doi.org/10.1007/s12403-016-0198-6

Li P, Wu J, Qian H (2016b) Preliminary assessment of hydraulic connectivity between river water and shallow groundwater and estimation of their transfer rate during dry season in the Shidi River, China. Environ Earth Sci 75(2):99. https://doi.org/10.1007/s12665-015-4949-7

Li P, Wu J, Qian H, Zhang Y, Yang N, Jing L, Yu P (2016c) Hydrogeochemical characterization of groundwater in and around a wastewater irrigated forest in the southeastern edge of the Tengger Desert, northwest China. Expo Health 8(3):331–348. https://doi.org/10.1007/s12403-016-0193-y

Li P, Wu J, Qian H (2016d) Hydrochemical appraisal of groundwater quality for drinking and irrigation purposes and the major influencing factors: a case study in and around Hua County, China. Arab J Geosci 9(1):15. https://doi.org/10.1007/s12517-015-2059-1

Li H, Bai HB, Wu JJ, Ma ZG, Ma K, Wu GM, Du YB, He SX (2017) A cascade disaster caused by geological and coupled hydro-mechanical factors–water inrush mechanism from karst collapse column under confining pressure. Energies 10(12):1938. https://doi.org/10.3390/en10121938

Li P, Wu J, Tian R, He S, He X, Xue C, Zhang K (2018) Geochemistry, hydraulic connectivity and quality appraisal of multilayered

groundwater in the Hongdunzi coal mine, northwest China. Mine Water Environ 37(2):222–237. https://doi.org/10.1007/s10230-017-0507-8

Li P, Tian R, Liu R (2019a) Solute geochemistry and multivariate analysis of water quality in the Guohua phosphorite mine, Guizhou Province, China. Expo Health 11(2):81–94. https://doi.org/10.1007/s12403-018-0277-y

Li P, He X, Li Y, Xiang G (2019b) Occurrence and health implication of fluoride in groundwater of loess aquifer in the Chinese Loess Plateau: a case study of Tongchuan, northwest China. Expo Health 11(2):95–107. https://doi.org/10.1007/s12403-018-0278-x

Liang YP, Gao XB, Zhao CH, Tang CL, Shen YY, Wang ZH, Wang YX (2018) Review: characterization, evolution, and environmental issues of karst water systems in northern China. Hydrogeol J 26(5):1371–1385. https://doi.org/10.1007/s10040-018-1792-4

Liu JT (2019) Hao Yj, Gao ZJ, Wang M, Liu MX, Wang ZY, Wang S (2019) Determining the factors controlling the chemical composition of groundwater using multivariate statistics and geochemical methods in the Xiqu coal mine, north China. Environ Earth Sci 78:364. https://doi.org/10.1007/s12665-019-8366-1

Liu P, Hoth N, Drebenstedt C, Sun Y, Xu Z (2017) Hydro-geochemical paths of multi-layer groundwater system in coal mining regions—using multivariate statistics and geochemical modeling approaches. Sci Total Environ 601–602:1–14. https://doi.org/10.1016/j.scitotenv.2017.05.146

Ma B, Jin M, Liang X, Li J (2018) Groundwater mixing and mineralization processes in a mountain-oasis-desert basin, northwest China: hydrogeochemistry and environmental tracer indicators. Hydrogeol J 26(1):233–250. https://doi.org/10.1007/s10040-017-1659-0

Qian H, Li P, Wu J, Zhou Y (2013) Isotopic characteristics of precipitation, surface and ground waters in the Yinchuan Plain, northwest China. Environ Earth Sci 70(1):57–70. https://doi.org/10.1007/s12665-012-2103-3

Qian H, Wu J, Zhou Y, Li P (2014) Stable oxygen and hydrogen isotopes as indicators of lake water recharge and evaporation in the lakes of the Yinchuan Plain. Hydrol Process 28:3554–3562. https://doi.org/10.1002/hyp.9915

Qian JZ, Wang L, Ma L, Lu YH, Zhao WD, Zhang Y (2016) Multivariate statistical analysis of water chemistry in evaluating groundwater geochemical evolution and aquifer connectivity near a large coal mine, Anhui, China. Environ Earth Sci 75(9):3–10. https://doi.org/10.1007/s12665-016-5541-5

Qian JZ, Tong Y, Ma L, Zhao WD, Zhang RG, He XR (2018) Hydrochemical characteristics and groundwater source identification of a multiple aquifer system in a coal mine. Mine Water Environ 37(3):528–540. https://doi.org/10.1007/s10230-017-0493-x

Rambabu S, Venkatesh AS, Syed TH, Surinaidu L, Srinivas P, Rai SP, Manoj K (2018) Stable isotope systematics and geochemical signatures constraining groundwater hydraulics in the mining environment of the Korba Coalfield, central India. Environ Earth Sci 77(15):2–17. https://doi.org/10.1007/s12665-018-7725-7

Richards LA, Magnone D, Boyce AJ, Casanueva-Marenco MJ, Dongen BE, Ballentine CJ, Polya DA (2018) Delineating sources of groundwater recharge in an arsenic-affected Holocene aquifer in Cambodia using stable isotope-based mixing models. J Hydrol 557:321–334. https://doi.org/10.1016/j.jhydrol.2017.12.012

Sefie A, Aris AZ, Ramli MF, Narany TS, Shamsuddin MKN, Saadudin SB, Zali MA (2018) Hydrogeochemistry and groundwater quality assessment of the multilayered aquifer in lower Kelantan Basin, Kelantan, Malaysia. Environ Earth Sci 77(10):397. https://doi.org/10.1007/s12665-018-7561-9

Shaw PJA (2003) Multivariate statistics for the environmental sciences. Hodder Arnold, London

Tomonaga Y, Marzocchi R, Pera S, Pfeifer HR, Kipfer R, Decrouy L, Vennemann T (2016) Using noble–gas and stable–isotope data to determine groundwater origin and flow regimes: application to the Ceneri Base Tunnel (Switzerland). J Hydrol 545:395–409. https://doi.org/10.1016/j.jhydrol.2016.11.043

Voutsis N, Kelepertzis E, Tziritis E, Kelepertsis A (2015) Assessing the hydrogeochemistry of groundwaters in ophiolite areas of Euboea Island, Greece, using multivariate statistical methods. J Geochem Explor 159:79–92. https://doi.org/10.1016/j.gexplo.2015.08.007

Wang D, Wu J, Wang Y, Ji Y (2019) Finding high–quality groundwater resources to reduce the hydatidosis incidence in the Shiqu County of Sichuan Province, China: analysis, assessment, and management. Expo Health. https://doi.org/10.1007/s12403-019-00314-y

Wu J, Li P, Qian H, Duan Z, Zhang X (2014) Using correlation and multivariate statistical analysis to identify hydrogeochemical processes affecting the major ion chemistry of waters: case study in Laoheba phosphorite mine in Sichuan. China. Arab J Geosci 7(10):3973–3982. https://doi.org/10.1007/s12517-013-1057-4

Wu J, Li P, Wang D, Ren X, Wei M (2019) Statistical and multivariate statistical techniques to trace the sources and affecting factors of groundwater pollution in a rapidly growing city on the Chinese Loess Plateau. Hum Ecol Risk Assess. https://doi.org/10.1080/10807039.2019.1594156

Xu C, Lu CH, Fan TY (2015) Analysis of the effect of mining coal on the water environment in the Panxie mining area of Huainan. Legisl Technol Pract Mine Reclam. https://doi.org/10.1201/b17500-8

Zhang X, Li X, Gao X (2016) Hydrochemistry and coal mining activity induced karst water quality degradation in the Niangziguan karst water system, China. Environ Sci Pollut Res 23(7):6286–6299. https://doi.org/10.1007/s11356-015-5838-z

Zhang HT, Xu GQ, Chen XQ, Mabaire Anesu (2019a) Hydrogeochemical evolution of multilayer aquifers in a massive coalfield. Environ Earth Sci 78:675. https://doi.org/10.1007/s12665-019-8694-1

Zhang HT, Xu GQ, Chen XQ, Wei J, Yu ST, Yang TT (2019b) Hydrogeochemical characteristics and groundwater inrush source identification for a multi-aquifer system in a coal mine. Acta Geol Sin 93(6):1922–1932. https://doi.org/10.1111/1755-6724.14299